Journal of Biomedical Optics

BiomedicalOptics.SPIEDigitalLibrary.org

Hemodynamic changes in a rat parietal cortex after endothelin-1-induced middle cerebral artery occlusion monitored by optical coherence tomography

Jian Liu
Yushu Ma
Shidan Dou
Yi Wang
Dongsheng La
Jianghong Liu
Zhenhe Ma

SPIE.

Jian Liu, Yushu Ma, Shidan Dou, Yi Wang, Dongsheng La, Jianghong Liu, Zhenhe Ma, "Hemodynamic changes in a rat parietal cortex after endothelin-1-induced middle cerebral artery occlusion monitored by optical coherence tomography," *J. Biomed. Opt.* **21**(7), 075014 (2016), doi: 10.1117/1.JBO.21.7.075014.

Hemodynamic changes in a rat parietal cortex after endothelin-1-induced middle cerebral artery occlusion monitored by optical coherence tomography

Jian Liu,[a] Yushu Ma,[a] Shidan Dou,[a] Yi Wang,[a] Dongsheng La,[a] Jianghong Liu,[b] and Zhenhe Ma[a,*]
[a]Northeastern University, School of Information Science and Engineering, No. 11 Lane Three Culture Road, Heping Area, Shenyang 110819, China
[b]Capital Medical University, Department of Neurology, Xuan Wu Hospital, No. 45 Changchun Street, Xicheng District, Beijing 100053, China

Abstract. A blockage of the middle cerebral artery (MCA) on the cortical branch will seriously affect the blood supply of the cerebral cortex. Real-time monitoring of MCA hemodynamic parameters is critical for therapy and rehabilitation. Optical coherence tomography (OCT) is a powerful imaging modality that can produce not only structural images but also functional information on the tissue. We use OCT to detect hemodynamic changes after MCA branch occlusion. We injected a selected dose of endothelin-1 (ET-1) at a depth of 1 mm near the MCA and let the blood vessels follow a process first of occlusion and then of slow reperfusion as realistically as possible to simulate local cerebral ischemia. During this period, we used optical microangiography and Doppler OCT to obtain multiple hemodynamic MCA parameters. The change trend of these parameters from before to after ET-1 injection clearly reflects the dynamic regularity of the MCA. These results show the mechanism of the cerebral ischemia-reperfusion process after a transient middle cerebral artery occlusion and confirm that OCT can be used to monitor hemodynamic parameters. [DOI: 10.1117/1.JBO.21.7.075014]

Keywords: optical coherence tomography; blood flow rate; middle cerebral artery occlusion; endothelin-1.

Paper 160223R received Apr. 9, 2016; accepted for publication Jul. 11, 2016; published online Jul. 29, 2016.

1 Introduction

The middle cerebral artery (MCA) on the cortical branch (M3 segment[1]) is one of the main sources of blood supply in the parietal cortex. Once blocked, it will seriously affect the oxygen supply of the cerebral cortex, resulting in irreversible nerve damage and brain function loss.[2] Changes in cerebral hemodynamic parameters in the MCA, such as vessel diameter, blood flow velocity, blood flow rate (BFR), and microvascular perfusion correlate strongly with the blood circulation of the cerebral cortex.[3] Therefore, measuring these changes can provide important information for therapy and rehabilitation after a middle cerebral artery occlusion (MCAO).[4]

Endothelin-1 (ET-1), which is secreted and released by vascular endothelial cells, is a potent vasoconstrictor on cerebral arteries in the vascular bed.[5] Following the topical application of ET-1 to the exposed MCA, there is a lasting and significant reduction in the BFR to pathological levels in the brains of rats.[6] After a period of time (determined by dose regulation), MCA will form a gradual reperfusion, which is very similar to a real stroke.[7] Therefore, the ET-1-induced MCA model has a distinct advantage over other models, such as cauterization, microclips and threads, intraluminal filaments, and photochemically induced thrombolytic occlusion.[8,9] However, the duration of reduced BFR and the reperfusion characteristics are poorly understood. Sharkey et al. used ET-1 to establish an early MCAO animal model. Fuxe et al. used laser Doppler to measure the decrease of BFR in the frontal and parietal lobe cortices after injecting ET-1 into a rat's brain cortex and observed the influence of different dosages. Filially, ET-1 enables a focal cerebral ischemia model.[10,11] If injected directly into the brain, ET-1 will have a profound and lasting influence on the BFR, which leads to ischemic brain damage around the MCA.[12,13] After ~20 to 30 min, the blood will gradually pass through the occluded vessels.[14,15] In addition to the above-mentioned research on the ET-1-induced MCAO model, there are still a number of phenomena and mechanisms to be studied.

Understanding the hemodynamic parameters after cerebral ischemia is critical. Many techniques have been used to measure these parameters, but some important limitations remain. Laser Doppler velocimetry[16] uses laser Doppler to measure the fluid velocity with high sensitivity and a wide dynamic range. However, it has the disadvantage of poor spatial resolution, which limits its ability to convey the overall morphology of microvascular perfusion.[15] Laser speckle contrast imaging (LSI)[17,18] has been used to detect changes in cerebral blood flow (CBF) in real time. Because of the spatial or temporal blurring of a speckle pattern from a laser onto a CCD camera, two-dimensional (2-D) maps of the CBF have high spatial and temporal resolution. However, because LSI lacks depth resolution, it cannot be used to determine the axial component of the blood vessels. Phase contrast magnetic resonance imaging (PC-MRI) uses the principle of bipolar gradient phase difference between the static structure and the fluid to carry out the quantitative measurement of flow rate based on the cross-sectional area of blood vessels to obtain BFR with no wound and no

*Address all correspondence to: Zhenhe Ma, E-mail: mazhenhe@163.com

1083-3668/2016/$25.00 © 2016 SPIE

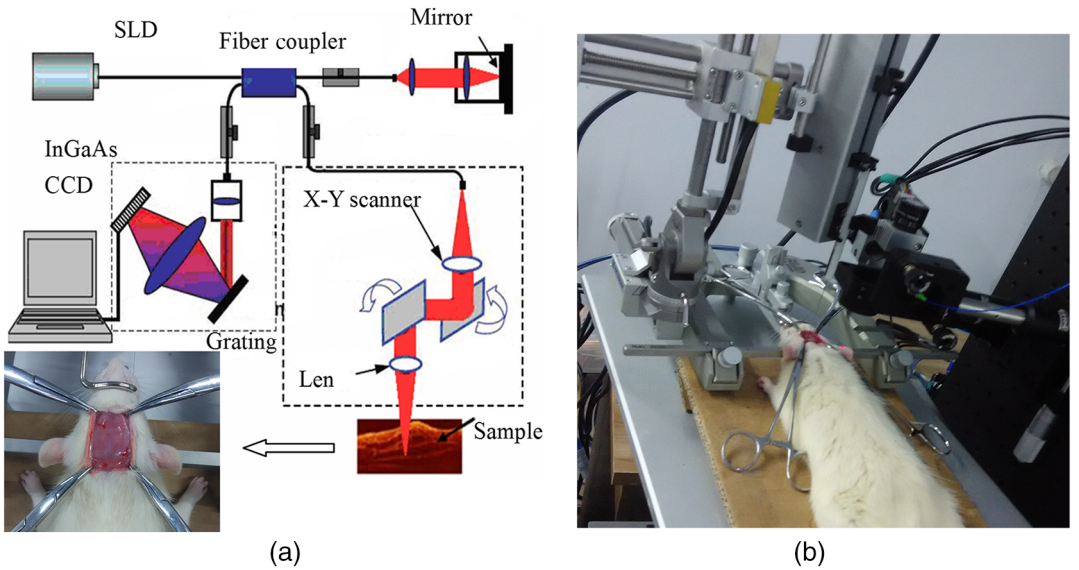

Fig. 1 (a) Schematic of our OCT system used to obtain hemodynamic MCA parameters. SLD: superluminescent diode, CCD: the charge coupled device. (b) Microinjection device for injecting ET-1.

depth limit. However, PC-MRI can have multiple errors and limited spatiotemporal resolution, which inevitably impact the accuracy of MRI-based hemodynamic parameter estimates.[19,20] In addition, the high cost of the equipment has limited the widespread use of PC-MRI. Transcranial Doppler (TCD) is an ultrasound technique based on the Doppler effect that can be used to study the hemodynamics of large intracranial blood vessels without a contrast agent and can accurately measure the axial blood flow velocity in some cerebral blood vessels.[21,22] TCD is commonly used to assess the collateral compensative capacity in patients with internal carotid artery occlusion.[23] There are, however, some disadvantages to high-frequency ultrasound for imaging hemodynamic MCA parameters. Although it is noninvasive, ultrasound requires the transducer to be in acoustic contact with the sample, and the appropriate acoustic window must be selected. Ultrasound is only capable of measuring the flow velocity of a limited number of large blood vessels. Its lateral resolution is not very satisfactory, and the measurement error of the Doppler angle is significant. To summarize, an accurate BFR measurement requires high temporal and spatial resolution, high sensitivity, and three-dimensional (3-D) imaging. To reduce the external stimulus and improve the accuracy, it also should be noncontact.

Optical coherence tomography (OCT) is a developing optical imaging technology based on the theory of partially coherent light interference, which has the potential to measure hemodynamic parameters in rats.[24] Chen et al.[25] combined OCT with Doppler technology and proposed phase-resolved Doppler OCT. This detects the axial displacement of blood cells at a specific time by measuring the phase difference ($\Delta\Phi$) between two adjacent A-scans and calculating the axial blood flow velocity of large blood vessels.[25–27] Wang et al.[28] first proposed a type of 3-D vascular reconstruction technology with high resolution which was based on OCT and was called optical microangiography (OMAG). It can separate the dynamic blood flow information from the static tissue and cannot only quantify the size of the vessel diameter, but also clearly show the orientation of the brain blood vessels. The latter is the prerequisite for the Doppler angle. The combination of the two techniques can be used to measure the BFR accurately and has been widely used. Zhi et al.[3] demonstrate the feasibility of OMAG and Doppler OCT and quantitatively assessed the retinal BFR in a rat model that had been subjected to raised intraocular pressure. Yali et al.[29] applied OMAG and the Doppler effect to study vascular microcirculation in mice under hypoxia, including the passive and active modulation of microvascular density and flux regulation. Baran et al.[4] applied the same technology to evaluate changes in vessel lumen diameter and blood flow velocity among a large number of pial and penetrating arterioles within the arteriolo-arteriolar anastomosis abundant region that overlays the penumbra in the parietal cortex after an MCAO. These findings reveal a number of important physiological mechanisms and have made significant contributions to human health. They also prove the efficacy of OCT in measuring hemodynamic parameters.

In this paper, we report on the use of OMAG and Doppler OCT to observe the process of MCA ischemia-reperfusion in a rat ischemia model induced by ET-1. We selected the MCA branches of the parietal cortex as a region of interest (ROI) to evaluate dynamic changes in blood vessel parameters (include diameter size, Doppler angle, and axial velocity) from before to after ET-1 injection. The absolute velocity of the blood can then be calculated by the Doppler angle and the axial velocity.[30] Finally, the diameter size and the absolute velocity will reflect the variation trend of BFR in the blood vessel.

2 System and Materials

2.1 *Systems*

This study employed a spectral domain optical coherence tomography system, which is based on an InGaAs line scan camera operating at a 79-kHz line rate [Fig. 1(a)]. This system utilizes a broadband superluminescent diode with 1321.5-nm central wavelength and 60-nm bandwidth to offer ~14 μm axial resolution in air. The ex-fiber output power was rated at ~8 mW. The light emitted from the light source was split into a sample arm and reference arm through a 2×2 fiber coupler. In the sample arm, the light was delivered to the sample through an optical probe containing a collimator, an *X*-*Y* 2-D galvanometer scanning system, and an objective lens. We used a 50-mm focal

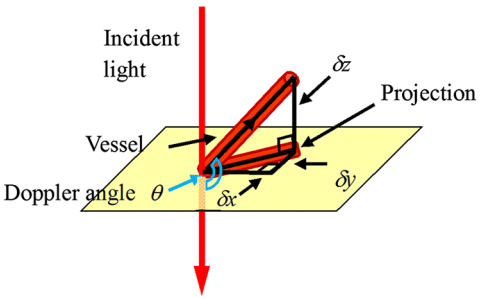

Fig. 2 Defined vessel Doppler angle.

length objective lens to achieve ~16-μm lateral resolution. The output light from the interferometer was routed to a home-built spectrometer, which consisted of a 30-mm focal length collimator, a 600 Grooves Grating (Edmund Optics Ltd.), and an achromatic focusing lens with 150-mm focal length. The focused light spectrum was impinged onto a line-scan CCD camera (Goodrich, 2048R). It had a designed spectral resolution of ~0.12 nm and provided a detectable depth range of ~3 mm on each side of the zero delay line. For OMAG imaging, we acquired 2 B-scans at each position to obtain dynamic information [Eq. (2)]. Totally, it takes ~1.5 s to achieve a 256×200 ($X \times Y$) OMAG image. When measuring the blood flow velocity, we acquired 200 B-scans at the same position. During one lateral B-scan cycle, 256 A-lines were acquired to cover ~1.1 mm on the ROIs. The overlap between adjacent two A-scans was about 75% (lateral diameter of sampling light focus point is ~16 μm), which was sufficient for Doppler spectral domain OCT measurement. The blood flow velocity shown in Fig. 2 is the average of 200 B-scans.

2.2 *Animal Models*

Three-month-old Sprague-Dawley rats (male) with body weights of ~250 g were used in this study. All procedures were performed in accordance with the Animal Ethics and Administrative Council of Northeastern University. All efforts were made to minimize animal suffering and to reduce the number of animals used. Surgical anesthesia was induced with sodium pentobarbital (3%, 5 mg/100 g, IP). The anesthetized rats were fixed on a stereotaxic apparatus (ST-5ND-C) with ear bars and a clamping device. The fur on the rats' heads was shaved, and the skin was cleaned with a 0.9% sodium chloride physiological solution. The skin was cut along the midline of the skull, and the interparietal bone was exposed by pulling the skin to the sides. Next, the subcutaneous tissue and the periosteum were cleaned. To obtain a clearer flow image, we ground the skull to a suitable thickness using a 1.2-mm diameter flat cranial drill. After the procedure, the rats were placed in the arm of the OCT sample and prepared for data acquisition [Fig. 1(b)]. The stereotaxic coordinates of the ET-1 injection were 2.59 mm anterior, 2.63 mm lateral, and 1.0 mm ventral relative to bregma. A 3-μl ET-1 (0.9% normal saline diluted to 100 pmol/L) dose was injected at 1 μl/ min. After injection, we waited for 3 min to ensure that the drug was fully absorbed. The needle was slowly removed, and the rat was immediately placed under the sample arm to begin scanning. This part of the procedure was performed using the translation table to ensure that the same position was used for every scan.

3 Methods and Theories

3.1 *Microvascular Perfusion Imaging*

Microvascular perfusion imaging based on OCT has extremely high resolution for perfusion imaging of the large blood vessels and clearly shows the distribution of microvascular perfusion. We were able to understand the cerebral cortex of the ischemic sample intuitively by observing the perfusion and distribution of nearby microblood vessels. This has significance for diagnosis and evaluation. When the infrared light passed through the sample, backscattering occurred at different depths, and the backscattered light received by the system can be regarded as the superposition of different depth components. The backscattered light and the reference light reflected by the plane mirror -generated interference. The interferogram of a B-scan captured by the CCD camera can be expressed as

$$I(k_i, t) = 2S(k_i)E_R\left[\int_{-\infty}^{\infty} a(z,t)\cos(2k_i n z)\mathrm{d}z\right], \quad (1)$$

where $i = 1 \ldots 1024$ is the pixel number index of the CCD camera; k_i is the wave number captured by the i'th pixel; t is the time point at which an A-scan is captured; E_R is the light reflected from the reference arm; $S(k)$ is the spectral density of the SLD light source used; $a(z,t)$ is the amplitude of the backscattered light at depth z; and n is the average refractive index of tissue, assumed to be constant.

A differential operation was applied to obtain dynamic information. This can be described as

$$I_j(k,t) = I(k, t + \Delta t_{\mathrm{B}}) - I(k,t), \quad j = 1,2,3,\ldots,200, \quad (2)$$

where $I_j(t,k)$ denotes the flow signal at j'th position (a total of 200 positions) along the C-scan direction and Δt_{B} is the time interval between adjacent B-scans. As the differential operation is equivalent to high-pass filtering, it suppressed the optical scattering signals from the static elements. Then, by applying fast Fourier transforms in k space, the solution to the depth direction was obtained. Finally, a 3-D microangiogram was rendered using Amira 3-D visualization software.

3.2 *Blood Flow Rate Measurement*

When the incident light is irradiating to the moving red blood cells, the frequency of the subsequent backscattering light will change due to the Doppler effect. If two adjacent A-scans are closely related, the phase difference ($\Delta\Phi$) between the two beams will introduce displacement, which can be expressed as

$$\Delta\varphi_{\mathrm{A}} = \frac{4\pi}{\lambda} n \Delta t_{\mathrm{A}} V_Z, \quad (3)$$

where λ is the central wavelength of the light source, n is the refractive index of tissue, and $\Delta t_{\mathrm{A}} = 1/79{,}000$ s is the time interval between adjacent A-scans. V_Z is the axial velocity, which can be expressed as

$$V_Z = \frac{\lambda \Delta\varphi_{\mathrm{A}}}{4\pi \Delta t_{\mathrm{A}}}. \quad (4)$$

To calculate the absolute velocity through the axial velocity, we needed to know the Doppler angle (the angle between the

incident light and the flow direction). The Doppler angle θ measurement equation for 3-D data is

$$\theta = \pi/2 + \arctan\left(\frac{\delta z}{\sqrt{\delta x^2 + \delta y^2}}\right), \tag{5}$$

where δ_x, δ_y, and δ_z are the distances between the three directions of 3-D data. $\sqrt{\delta x^2 + \delta y^2}$ represents the length of the vessel's projection in the X-Y plane.

Absolute flow velocity V can be expressed as

$$V = \left|\frac{V_z}{\cos\theta}\right|. \tag{6}$$

Blood vessel diameter was calculated by the boundary of the vessel's contour in the OCT blood vessel image. The cross-sectional area of the blood vessel can be calculated using $S = \pi(D/2)^2$.

The BFR was then calculated by multiplying the absolute average velocity $\overline{V}$ by the cross-sectional area S of the blood vessel

$$\mathrm{BFR} = \overline{V} \cdot S. \tag{7}$$

4 Results

Figure 3(a) shows a vascular network of the entire cerebral cortex of rat 1 with an image size of 7.5 mm × 8.5 mm × 1.5 mm. It is made up of 12 sub-images, each sub-image was 2.5 mm × 2.5 mm × 1.5 mm with 256 × 200 A-scans. The ultrahigh resolution ability of OCT angiography can show the distribution of rat cerebral microvascular networks and accurately determine the ROI. The green label of the black arrow is the selected injection location of ET-1. A small hole was drilled at that location with a hand-held cranial drill. The white box shows the ROI, whose size is 1.2 mm × 1.2 mm × 1.5 mm; the voxel number is 256 × 200 × 512. Figures 3(b)–3(j) show the change of the blood vessel diameter from before to after ET-1 injection in the ROI. The data were collected every 5 min for a total of 10 measurements. The diameter of the blood vessels first began to decrease, reached a minimum at 10 min, and recovered slowly. Mecca at al. observed primary and secondary branches of the MCA during ET-1injection using a microscope and described the changes of blood vessel diameter over time. That study included a sham operation group, a normal control group, and a drug intervention group.[31] The variations in diameter in this paper are consistent with those in Ref. 31.

Figures 4(a)–4(c) show blood vessel perfusion maps of three rats in the ROI prior to the injection of ET-1. The white arrow indicates each MCA branch to be measured, and the white line is the cross-section of the velocity measurement. Figure 4(d) is the change curve of each MCA diameter.

Figure 5 shows the acquisition process of the Doppler angle. We obtained a 3-D vasculature image [Fig. 5(a)] using OMAG. To demonstrate the MCA's Doppler angle calculation method more clearly, we separated the blood vessels shown in Fig. 5(a) and projected them in the X-Y [Fig. 5(b)] and the Y-Z [Fig. 5(c)] planes to determine the projection length of the MCA in the X-Y plane $\sqrt{\delta x^2 + \delta y^2}$ and the projection height in the Y-Z plane δ_z. In this paper, these physical quantities are 1 and 0.2 mm, respectively. The Doppler angle calculated by Eq. (5) was ~101.3 deg.

The next step was to calculate the absolute blood flow velocity of the MCA, which was divided into three steps. First, the phase difference was measured by OCT Doppler. The axial velocity V_Z was then obtained by Eq. (4). Finally, the absolute velocity was obtained using Eq. (6). Here, all pixel values were positive because we used the modulus. Quantitative results for each step are shown in Table 1. Figure 6 shows the average absolute velocity of rat 1 at different times. There is an obvious

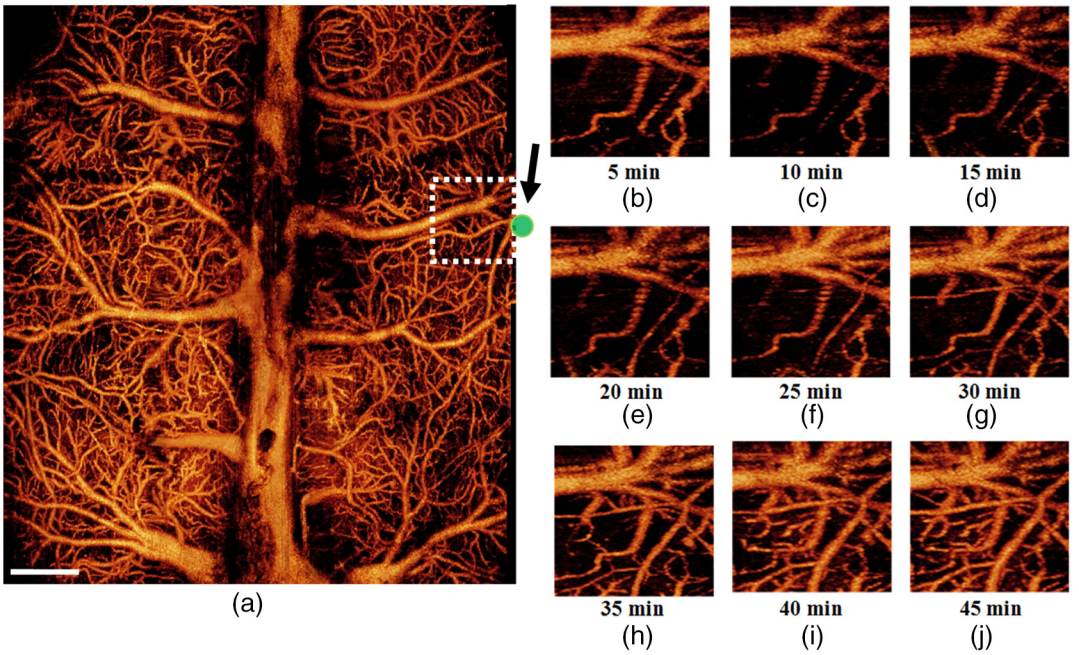

Fig. 3 Changes in blood vessel diameter of rat 1. (a) Whole brain blood vessel image, the position of the green label is the location of the ET-1. The white box is the MCA parameter acquisition area (i.e., ROI). (b–j). The change of the blood vessel diameter from before to after ET-1 injection.

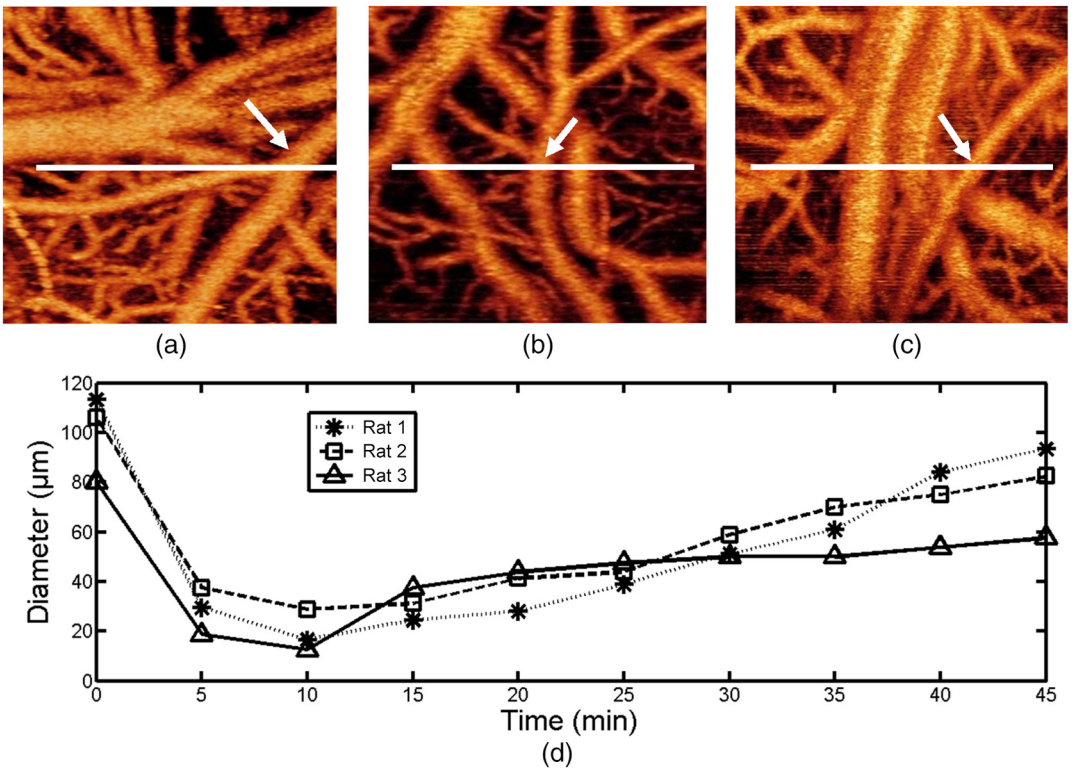

Fig. 4 Changes of blood vessel diameter from before to after ET-1 injection. (a–c) Vascular images prior to injection. The white arrows indicate the vessel to be measured, the white line marks the position of velocity measurement (B-scan). (d) Blood vessel diameter change curve.

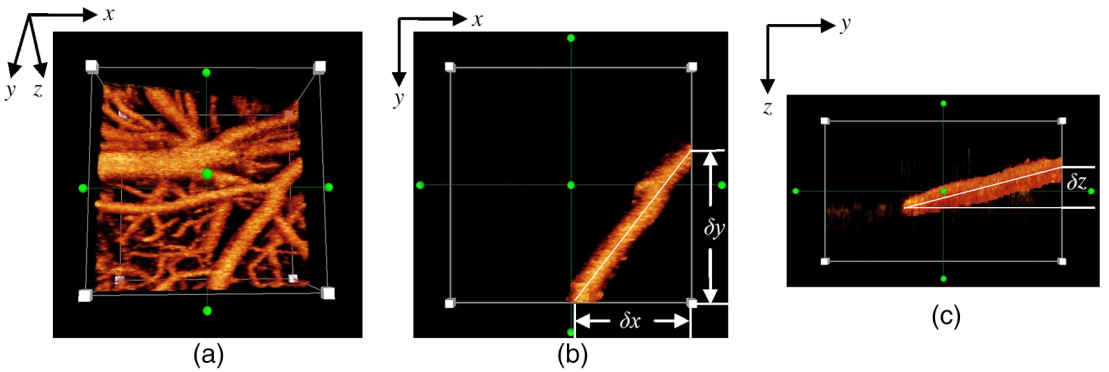

Fig. 5 Schematic diagram of the acquisition method of Doppler angle. (a) 3-D vasculature image showing the vessel orientation. (b) The projection of MCA in x-y plane to calculate the length $\sqrt{\delta x^2 + \delta y^2}$. (c) The projection of MCA in x-y plane to calculate the height δ_z.

difference between Figs. 6(b) and 6(a). The value shown in Fig. 6(e) is approximately half at the same time point (0 min).

Figure 7(a) shows the absolute velocity change curve of the MCA, which was calculated using Eq. (6). The trends of the blood vessel diameter change and variation of absolute velocity are extremely close, as shown in Figs. 4(d) and 7(a), indicating that ET-1 can effectively shrink blood vessels and block blood flow. Figure 7(b) shows the instantaneous absolute velocity curve of rat 1 at the MCA center at time (0 min) and (10 min). The abscissa is the number of B-scans. In this paper, each group of data was collected from 200 B-scans, and each B-scan contained 256 A-scans. The sampling time of each group of data was 1 s. As is shown in Fig. 7(b), the heart rate of rats is ~6 beats/s. At time point 10, the blood flow velocity can be negative, which indicates that the flow direction has changed. Figure 7(c) shows the change of the BFR. After ~45 min, the MCA diameter returned to ~80% of their initial state, the absolute velocity returned to half of their initial state, and the BFR returned to only 30% to 40% of their initial state.

5 Discussion

This paper uses a vasoconstrictor substance called ET-1 to construct a rat focal cerebral ischemia model, and the model was monitored in real time using OCT. Some meaningful cerebral hemodynamic parameters were obtained. These results not only reflect the mechanism of ET-1 in the cerebral blood vessels, but also proved that OCT has the ability to observe the changes

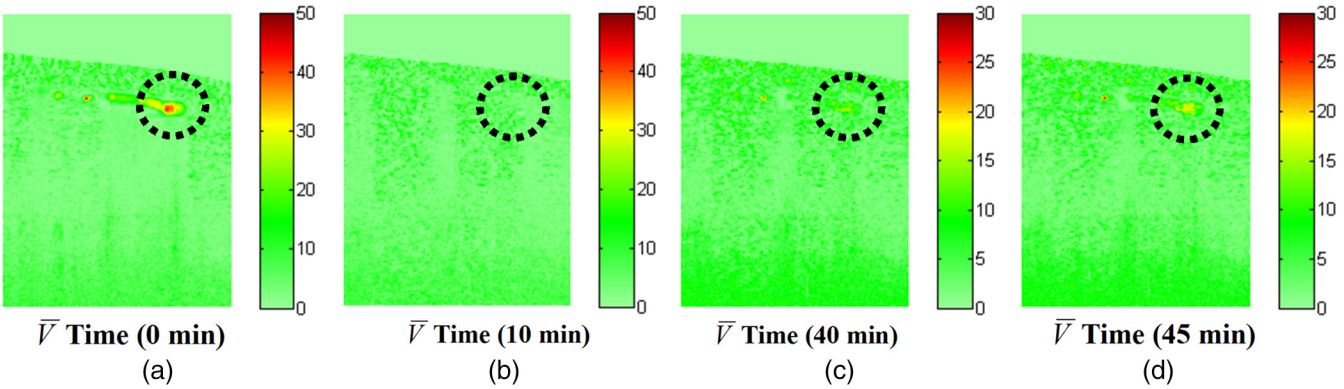

Fig. 6 B-scan of average absolute velocity of rat 1 at the times of (0 min), (10 min), (40 min), and (45 min).

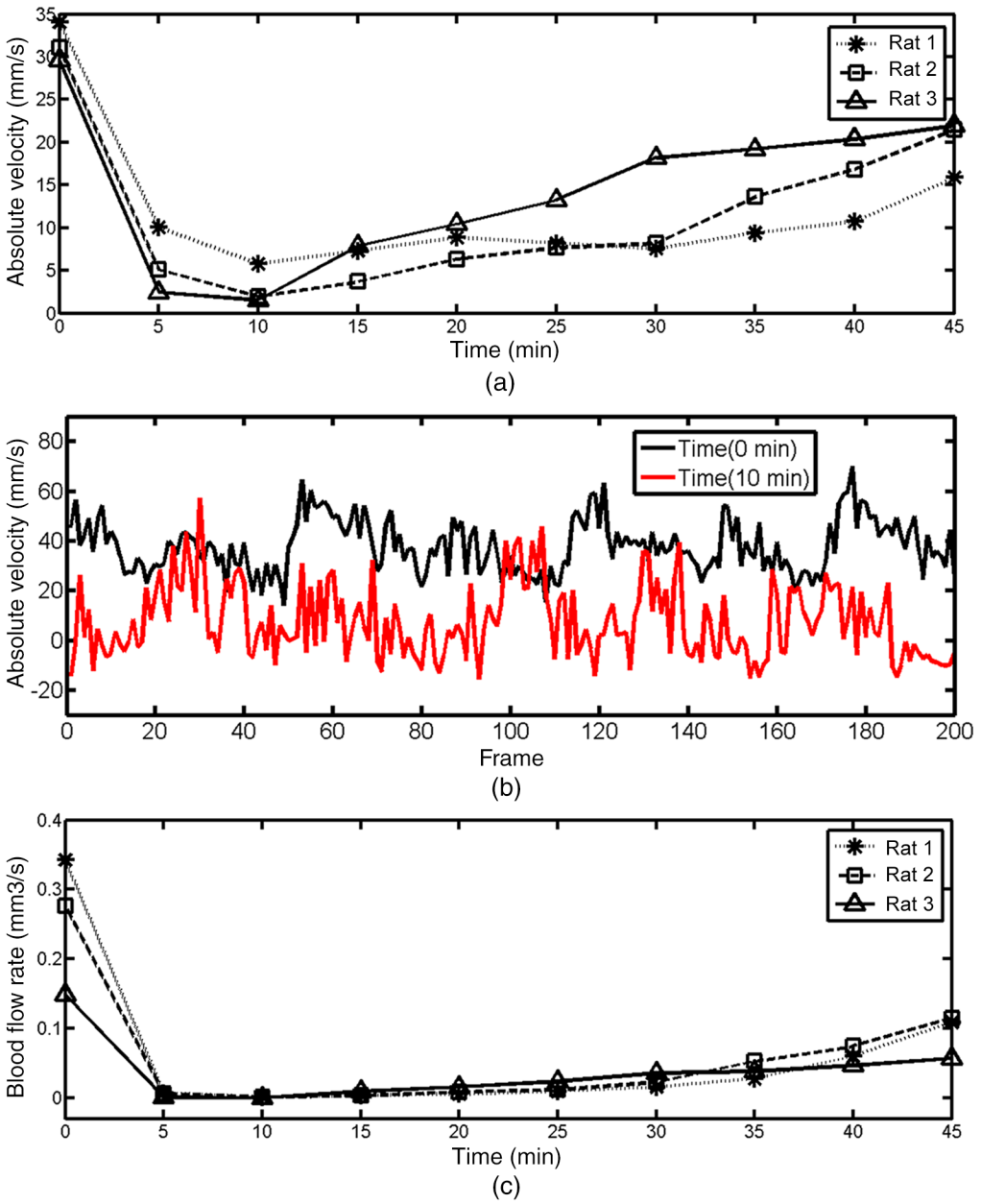

Fig. 7 (a) Average absolute velocity change curve of MCA. (b) Instantaneous absolute velocity of rat 1 at (time 0) and (time 10). The abscissa is the number of B-scan. (c) BFR change curve.

Table 1 Quantitative results of the hemodynamic parameters for the MCA at different times.

Time	$\overline{\Delta\varphi_A}$ (rad)	$\overline{V_Z}$ (mm/s)	Doppler angle (deg)	$\overline{V}$ (mm/s)	Diameter (μm)	BFR (mm^3/s)
Rat 1						
0 min	−0.79	−6.59	101.3	33.63	113.2	0.338
10 min	−0.13	−1.09		5.545	16.5	0.0012
40 min	−0.27	−2.26		10.96	84.08	0.0609
45 min	−0.373	−3.10		15.80	93.4	0.108
Rat 2						
0 min	−0.51	−4.22	97.8	31.1	106.3	0.28
10 min	−0.03	−0.27		1.95	28.75	0.0013
40 min	−0.28	−2.29		16.84	75.0	0.074
45 min	−0.35	−2.91		21.45	82.5	0.115
Rat 3						
0 min	−1.36	−11.27	112.4	29.58	80.0	0.16
10 min	−0.07	−0.58		1.52	12.5	0.0002
40 min	−0.93	−7.75		20.34	53.75	0.046
45 min	−1.01	−8.35		21.9	57.5	0.057

Note: "−" indicates that the direction of blood flow is oriented to the direction of the beam.

of hemodynamics in the cerebral blood vessels after regulation by the hormone substance.

The MCA branches are the main sources of blood supply in the parietal cortex of the brain. The blockage of this vessel will seriously affect the blood supply to the cerebral cortex, resulting in irreversible nerve damage and brain function loss. Therefore, the injection site is near the upstream of the MCA branches. Injecting ET-1 1 mm into the cortex can most directly induce the ischemia-reperfusion process. Of course, ET-1 can also be injected at other locations of the brain, such as the white matter, striatum, and proximal cerebral artery, to produce a model that meets the requirements.[32] The concentration of ET-1 in this experiment was 100 pmol/μl. We obtained the ischemia model with a 10-min occlusion and ∼1 h of reperfusion. The times of occlusion and reperfusion differ depending on the ET-1 dose and corresponding antibodies that are regulated.[33]

A whole brain blood vessel distribution map covering all cortical regions is critical because it can help determine the MCA parameter acquisition area (i.e., ROI), as shown in Fig. 3. The shrinkage degree of blood vessels from before to after ET-1 injection has been described in detail. An MCA blockage severely affects the blood supply of the cerebral cortex. Most of the capillaries in the ROI are not shown in Figs. 3(b)–3(f). This indicates that the blood flow in the capillaries is stopped or that blood flow velocity is too low, leaving the cortex in the ROI in a state of ischemia and hypoxia. Because of the slow blood flow velocity, the blood vessels in the figure are discontinuous. When the blood flows in the diastolic heart, the flow signal is lost because the blood flow velocity is reduced to the lowest value, which is beyond the sensitivity range of the system. When the blood flows in the systolic heart, the gradual recovery of the flow velocity brings the flow signal. Occasional vasospastic responses may be another cause of vascular discontinuity. After ∼30 min, the capillaries begin to gradually recover. In this time period, the brain's cortex is likely to have been severely damaged.

ET-1 is the most potent vasoconstrictor on cerebral arteries to be identified to date. It induces the blood vessels to shrink to nearly a closed state in a short time, which severely affects the blood flow velocity in the downstream blood vessels. Therefore, the change in MCA diameter is the direct effect of ET-1, while the change in MCA flow velocity is due to upstream obstruction. As is shown in Figs. 4(d) and 7(a), the change trends of the MCA blood vessel diameter and absolute velocity are synchronous. This phenomenon illustrates two things. The range of action of ET-1 is great as it both blocks the point of injection and shrinks the MCA in an ROI. In addition, the diffusion speed of ET-1 is very fast, as shown by the fact that the injection point and ROI response are almost simultaneous. It is worth noting that the velocity/BFR showed a much delayed recovery compared to the recovery of vessel diameter. After 45 min, the MCA diameter returned to ∼80% of its initial state and the absolute velocity to only half of its initial state. This is probably caused by ischemia reperfusion injury-induced vascular endothelial dysfunction, which is largely a consequence of changes in the endothelial cells themselves, affecting the integrity of barrier function, cytokine and adhesion molecule expression, and vascular tone.[34] Impaired blood vessels are difficult to recover in the short term. Therefore, the blood flow cannot be restored to the level before the vascular occlusion. Because of individual differences, there are some differences in reperfusion injury in different rats. The speed of blood flow recovery was proportional to the degree of injury. It can be seen from Fig. 7(a) that the recovered blood flow velocities of rat 2 and rat 3 were faster than that of rat 1. Figure 7(b) shows that the value of absolute velocity of rat 1 at time point 10 hovered near zero, indicating that the flow direction of some adjacent vessels can be changed after severe stenosis or occlusion and that the appearance of pathological channels can be identified according to the changes in blood flow direction. After 45 min, the BFR remained at a low level for a long time, confirming that the model mimics a stroke [Fig. 7(c)].

Two more samples of rats have been used to demonstrate the ability to reproduce these experiments. As can be seen from the results, it is obvious that the hemodynamic parameters of the three rats reached the lowest point after 10 min of the injection, and then gradually recovered. Depending on individual differences, the degree of recovery is slightly different, but the overall change trend is similar.

6 Conclusion

This paper shows the mechanism of cerebral ischemia-reperfusion after ET-1-induced MCAO. After an ET-1 injection, the BFR will first decline rapidly and then slowly recover. This is significant for drug development and other basic research. This paper also proves the efficacy of OCT in blood flow monitoring, providing an important reference for therapy and rehabilitation after MCAO.

Acknowledgments

This work was supported in part by National Natural Science Foundation of China (31170956, 61501100, 81301208, and 61275214), Hebei Provincial Natural Science Foundation of China (A2015501002 and H2015501133). Fundamental Research Funds for the Central Universities (N120223001), Research Fund for Higher School Science and Technology in Hebei Province (QN20132014), Science and Technology Research and Development project funds of Shenzhen (JCYJ20120618142137681), and the Colleges and Universities Scientific Research projects in Hebei Province (Z2015207).

References

1. E. J. Roth, "Middle cerebral artery," in *Encyclopedia of Clinical Neuropsychology*, pp. 57–65, Springer, New York (2011).
2. G. J. Rubino and W. Young, "Ischemic cortical lesions after permanent occlusion of individual middle cerebral artery branches in rats," *Stroke* **19**(7), 870–877 (1988).
3. Z. W. Zhi et al., "Volumetric and quantitative imaging of retinal blood flow in rats with optical microangiography," *Biomed. Opt. Express* **2**(3), 579–591 (2011).
4. U. Baran, Y. Li, and R. K. Wang, "Vasodynamics of pial and penetrating arterioles in relation to arteriolo-arteriolar anastomosis after focal stroke," *Neurophotonics* **2**, 025006 (2015).
5. M. Yanagisawa et al., "A novel potent vasoconstrictor peptide produced by vascular endothelial cells," *Nature* **332**(6163), 411–415 (1988).
6. K. Fuxe et al., "Endothelin-1 induced lesions of the frontoparietal cortex of the rat. A possible model of focal cortical ischemia," *Neuroreport* **8**(11), 2623–2629 (1997).
7. C. F. Chang et al., "Hyperbaric oxygen therapy for treatment of postischemic stroke in adult rats," *Exp. Neurol.* **166**(2), 298–306 (2001).
8. R. G. Robinson et al., "Effect of experimental cerebral infarction in rat brain on catecholamines and behavior," *Nature* **255**(5506), 332–334 (1975).
9. S. Moyanova, R. Kirov, and L. Kortenska, "Multi-unit activity suppression and sensorimotor deficits after endothelin-1-induced middle cerebral artery occlusion in conscious rats," *J. Neurol. Sci.* **212**(1–2), 59–67 (2003).
10. J. Sharkey, I. M. Ritchie, and P. A. Kelly, "Perivascular microapplication of endothelin-1: a new model of focal cerebral ischaemia in the rat," *J. Cerebral Blood Flow Metab.* **13**(5), 865–871 (1993).
11. K. Fuxe et al., "Endothelin-1 induced lesions of the frontoparietal cortex of the rat. a possible model of focal cortical ischemia," *Neuroreport* **8**(11), 2623–2629 (1997).
12. K. Fuxe et al., "Involvement of local ischemia in endothelin-1 induced lesions of the neostriatum of the anaesthetized rat," *Exp. Brain Res.* **88**(1), 131–139 (1992).
13. J. L. Reid, D. Dawson, and I. M. Macrae, "Endothelin, cerebral ischaemia and infarction," *Clin. Exp. Hypertens.* **17**(1–2), 399–407 (2009).
14. I. M. Macrae et al., "Endothelin-1-induced reductions in cerebral blood flow: dose dependency, time course, and neuropathological consequences," *J. Cerebral Blood Flow Metab.* **13**(2), 276–284 (1993).
15. S. Nikolova, "Endothelin-1 induced MCAO: dose dependency of cerebral blood flow," *J. Neurosci. Methods* **179**(1), 22–28 (2009).
16. C. P. Wang, "Laser Doppler velocimetry," *J. Quantum Spectrosc. Radiat. Transfer* **40**(3), 309–319 (1988).
17. A. Ponticorvo et al., "Imaging hemodynamic effects of et-1 on cerebral blood flow in rats," *Proc. SPIE* **6446**, 64460U (2007).
18. J. Qin et al., "Hemodynamic and morphological vasculature response to a burn monitored using a combined dual-wavelength laser speckle and optical microangiography imaging system," *Biomed. Opt. Express* **3**(3), 455–466 (2012).
19. V. C. Rispoli et al., "Computational fluid dynamics simulations of blood flow regularized by 3D phase contrast MRI," *Biomed. Eng. Online* **14**(1), 1–23 (2015).
20. A. Harlof et al., "*In vivo* assessment of wall shear stress in the atherosclerotic aorta using low-sensitive 4D MRI," *Magn. Reson. Med.* **63**(6), 1529–1536 (2010).
21. M. A. Moehring et al., "Doppler ultrasound method and apparatus for monitoring blood flow and hemodynamics," Patent No. EP US 7,128,713 (2006).
22. N. Yagi et al., "Noninvasive diagnosis of blood flow for transcranial doppler ultrasonography," *Int. J. Intell. Comput. Med. Sci. Image Process.* **5**(1), 67–79 (2013).
23. X. W. Zhang, J. Y. Niu, and M. U. Pei-Yuan, *Collateral Compensative Capacity Assessed by Transcranial Doppler in Aged Patients with Internal Carotid Artery Occlusion*, Editorial Department of Chinese Journal of Geriatric Cardiovascular & Cerebrovascular Disease (2005).
24. D. Huang et al., "Optical coherence tomography," *Science* **254**(5035), 1178–1181 (1991).
25. Z. P. Chen et al., "Noninvasive imaging of *in vivo* blood flow velocity using optical Doppler tomography," *Opt. Lett.* **22**(14), 1119–1121 (1997).
26. J. Zhang and Z. Chen, "*In vivo* blood flow imaging by a swept laser source based Fourier domain optical Doppler tomography," *Opt. Express* **13**(19), 7449–7457 (2005).
27. R. A. Leitgeb et al., "Real-time assessment of retinal blood flow with ultrafast acquisition by color Doppler Fourier domain optical coherence tomography," *Opt. Express* **11**, 3116–3121 (2003).
28. R. K. Wang et al., "Three dimensional optical angiography," *Opt. Express* **15**, 4083 (2007).
29. J. Yali, L. Peng, and R. K. Wang, "Optical microangiography provides an ability to monitor responses of cerebral microcirculation to hypoxia and hyperoxia in mice," *J. Biomed. Opt.* **16**(9), 480–484 (2011).
30. A. Davis, J. Izatt, and F. Rothenberg, "Quantitative measurement of blood flow dynamics in embryonic vasculature using spectral Doppler velocimetry," *Anat. Rec. (Hoboken)* **292**(3), 311–319 (2009).
31. A. P. Mecca et al., "Candesartan pretreatment is cerebroprotective in a rat model of endothelin-1-induced middle cerebral artery occlusion," *Exp. Physiol.* **94**(8), 937–946 (2009).
32. J. Sharkey, I. M. Ritchie, and P. A. Kelly, "Perivascular microapplication of endothelin-1: a new model of focal cerebral ischaemia in the rat," *J. Cerebral Blood Flow Metab.* **13**(5), 865–871 (1993).
33. S. Nikolova, "Endothelin-1 induced MCAO: dose dependency of cerebral blood flow," *J. Neurosci. Methods* **179**(1), 22–28 (2009).
34. J. B. Seal and B. L. Gewertz, "Vascular dysfunction in ischemia-reperfusion injury," *Ann. Vasc. Surg.* **19**(19), 572–584 (2005).

Zhenhe Ma completed his PhD in 2007. He is a associate professor at Northeastern University at Qinhuangdao, China. He did postdoctoral research at Oregon Health and Science University from 2009 to 2010. His main research directions are optical coherence tomography, infrared spectroscopy, and Raman spectroscopy.

Biographies for the other authors are not available.